COMPDYN 2015
5th ECCOMAS Thematic Conference on
Computational Methods in Structural Dynamics and Earthquake Engineering
M. Papadrakakis, V. Papadopoulos, V. Plevris (eds.)
Crete Island, Greece, 25–27 May 2015

INCREMENTAL DYNAMIC ANALYSIS OF FIRE-EXPOSED BASE-ISOLATED R.C. FRAMED BUILDINGS SUBJECTED TO NEAR-FAULT GROUND MOTIONS

Fabio Mazza[1] **and Fabio Alesina**[2]

[1]Dipartimento di Ingegneria Civile, Università della Calabria
Via P. Bucci, 87036 Rende (CS), Italy
fabio.mazza@unical.it

[2]Dipartimento di Ingegneria Civile, Università della Calabria
Via P. Bucci, 87036 Rende (CS), Italy
fabioalesina@yahoo.it

Keywords: Base-Isolated Structures, Fire Scenarios, Thermal Mappings, Near-Fault Ground Motions, Incremental Dynamic Analysis.

Abstract. *It is well known that near-fault ground motions are characterized by long-duration horizontal pulses, which can become critical for base-isolated reinforced concrete (r.c.) structures when the pulse intensity is so strong that the superstructure undergoes plastic deformations. There is, however, a lack of knowledge on the seismic response in case of fire; moreover, an amplification of the structural damage is expected in case of fire-exposed base-isolated structures which are not designed to withstand fire. To investigate the nonlinear seismic response following a fire, an incremental dynamic analysis is carried out with reference to five-storey base-isolated r.c. buildings with fire-protected High-Damping-Laminated-Rubber Bearings (HDLRBs), designed according to the Italian seismic code. Horizontal components of seven near-fault ground motions have been selected according to the design subsoil class C adopted for the test structures. More specifically, the nonlinear seismic response of base-isolated structures in a no fire situation is compared with that in which fire occurs, at 45 (i.e. R45) and 60 (i.e. R60) minutes of fire resistance, assuming both damaged (i.e. DS) and repaired (i.e. RS) stiffness conditions. Five fire scenarios are considered assuming the fire compartment confined to the area of the first level (i.e. F1), the first two (i.e. F1/2) and the upper (i.e. Fi, i=3-5) levels, with the parametric temperature-time fire curve evaluated according to Eurocode 1. The nonlinear seismic analysis is performed by using a step-by-step procedure based on a two-parameter implicit integration scheme and an initial-stress-like iterative procedure. At each step of the analysis, plastic conditions are checked at the critical (end) sections of the girders and columns, where thermal mapping with reduced mechanical properties is evaluated with the 500°C isotherm method proposed by Eurocode 2. A viscoelastic model with variable stiffness properties in the horizontal and vertical directions, depending on the axial force and lateral deformation, simulates the response of an HDLRB.*

1 INTRODUCTION

Fire can be a serious problem for a structure that has been partially damaged in a prior seismic event, because fire resistance will decrease with respect to an undamaged structure [1]. Recent studies have focused the attention on the combined effect of earthquake and fire on the nonlinear response of reinforced concrete (r.c.) [2, 3], steel [4, 5] and composite steel-concrete [6] fixed-base structures. On the other hand, numerical [7] and experimental [8, 9] studies have been carried out on the residual seismic load capacity of fixed-base structures, in terms of stiffness, strength and ductility after fire. In most of cases of fire, framed structures experience degradation of material properties, due to the high temperature, and damage to the structural members, from thermal expansion. There is, however, a lack of knowledge on the seismic response of base-isolated structures in case of fire and an amplification of the structural damage is expected in the case of fire-exposed base-isolated structures not designed to withstand fire.

When a base-isolated structure is designed for a sufficiently high strength level, it behaves elastically and the vibration periods of the upper framed structure are shorter than the predominant periods of the motion filtered by the isolators. Nevertheless, the frequency content of the motion transmitted by the isolators to the superstructure can become critical as soon as the strength level of a fire-weakened base-isolated structure is reduced; as a consequence, the superstructure can undergo plastic deformations and the ductility demand can increase much more rapidly for an ever-lower strength level. Moreover, a considerable increase in the deformability of a base-isolated structure, in comparison with that of the corresponding fixed-base structure, may lead to an amplification in the structural response under near-fault ground motions [10, 11], which are characterized by long-duration (horizontal) directivity and fling-step pulses due to fault-rupture directivity and elastic rebound effects, respectively [12].

In the present work, the nonlinear seismic response of base-isolated structures in a no fire situation is compared with that in which fire occurs, at 45 (i.e. R45) and 60 (i.e. R60) minutes of fire resistance, assuming both damaged (i.e. DS) and repaired (i.e. RS) stiffness conditions in the r.c. frame members. To this end, five-storey r.c. office buildings, base-isolated with fire-protected High-Damping-Laminated-Rubber Bearings (HDLRBs), are designed according to the Italian seismic code [13]. A numerical fire investigation is carried out considering a thermal-mechanical mapping analysis, with reduced mechanical properties evaluated according to the 500°C isotherm method proposed by Eurocode 2 [14], followed by a sequentially uncoupled nonlinear incremental dynamic analysis. Horizontal components of seven near-fault ground motions, available in the *Pacific Earthquake Engineering Research center database* [15] and corresponding to both directivity and fling-step pulse-type records, are selected according to the design subsoil class C adopted for the test structures [16]. Five fire scenarios have been considered assuming the fire compartment is confined to the area of the first level (i.e. F1), the first two (i.e. F1/2) and the upper (i.e. Fi, i=3-5) levels, with the parametric temperature-time fire curve evaluated according to Eurocode 1 [17].

2 LAYOUT AND DESIGN OF THE BASE-ISOLATED R.C. FRAMED BUILDING

A typical five-storey office building with an r.c. framed structure isolated at the base by fifteen identical fire-protected HDLRBs is considered for the numerical investigation. The symmetric plan of the building and the elevation of a base-isolated plane frame are shown in Figures 1a and 1b, respectively, where length and cross-sections of the frame members are also shown. Perimeter masonry infills, assumed as non-structural elements regularly distributed in elevation, are considered (Figure 1a). A grid of rigid girders is placed at the base of the framed structure on the HDLRBs (Figure 1b). For the sake of simplicity, the plane frames ori-

entated along the horizontal ground motion direction (y), perpendicular to the floor slab direction (x) shown in Figure 1a, are considered as a reference scheme. Five fire scenarios are reported in Figures 1a and 1c, assuming the fire compartment is confined to the area of the first level (i.e. F1), the first two (i.e. F1/2) and the upper (i.e. Fi, i=3-5) levels.

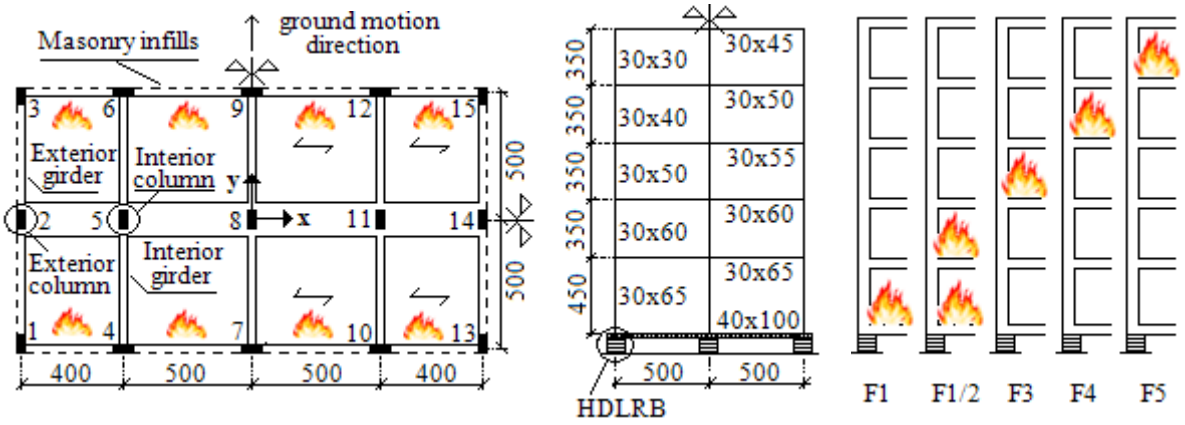

(a) Plan and fire compartment. (b) Elevation. (c) Fire scenarios.

Figure 1: Base-isolated r.c. test structure (dimensions in cm).

The proportioning of the test structure has been done according to the Italian seismic code (NTC08) assuming, besides the gravity loads, the horizontal seismic loads corresponding to: elastic response of the superstructure (behaviour factor q=1); design subsoil class C (subsoil parameter S=1.41); high-risk seismic region (peak ground acceleration, PGA=0.201gx1.41 =0.283g). The acceleration design spectrum is modified in the period range $T \geq 0.8T_{I,H}$, being $T_{I,H}$ the fundamental vibration period of the base-isolated structure in the horizontal direction, assuming an equivalent viscous damping ratio of the isolation system $\xi_{I,H}$=10%, at shear deformation γ=1. Moreover, NTC08 requires that $3T_{F,H} \leq T_{I,H} \leq 3$s, $T_{F,H}$ being the fundamental vibration period of the same structure on fixed-base. In the present case a reasonable isolation period was $T_{I,H}$=2.5 s having $T_{F,H}$=0.73 s; an isolation degree, in terms of spectral acceleration at the fundament vibration period, equal to α_{Sa}=0.28(=$S_{a,I}/S_{a,F}$) is obtained. Finally, the vibration period with prevailing component in the vertical direction is $T_{I,V}$=0.072 s with the corresponding equivalent viscous damping ratio $\xi_{I,V}$=2%.

The gravity loads used in the design are represented by dead- and live loads, equal respectively to: 4.4 kN/m^2 e 3 kN/m^2, for the top floor; 6.1 kN/m^2 e 3 kN/m^2, for the isolated floor; 5.7 kN/m^2 e 3 kN/m^2, for the other floors. The weight of the perimeter masonry infills is taken into account by considering a gravity load of 2.7 kN/m^2. A cylindrical compressive strength of 25 N/mm^2 for the concrete and a yield strength of 450 N/mm^2 for the steel are assumed for the r.c. frame members. The design of the superstructure has been carried out so as to satisfy minimum conditions for the longitudinal bars of the girders and columns, according to the provisions for low ductility class imposed by NTC08: at least two 14 mm bars are provided both at the top and bottom throughout the entire length of all the frame members; for the girders, a tension reinforcement ratio not less than 0.31% (for the assumed yield strength) is provided and a compression reinforcement not less than half of the tension reinforcement is placed at their end sections; a minimum steel geometric ratio of 1% is assumed for the symmetrically-reinforced section of each column.

The HDLRBs fulfill the ultimate limit state verifications regarding the maximum shear strains: i.e. $\gamma_{tot}=\gamma_s+\gamma_c+\gamma_\alpha \leq 5$ and $\gamma_s \leq 2$, where γ_{tot} represents the total design shear strain, while γ_s, γ_c and γ_α represent the shear strains of the elastomer due to seismic displacement, axial

compression and angular rotation, respectively. Moreover, the maximum compression axial load (P) does not exceed the critical load (P_{cr}) divided by a safety coefficient equal to 2.0. The minimum tensile stress (σ_t) resulting from the seismic analysis is assumed as $2G$(=0.8 MPa, for a shear modulus of the elastomer G=0.4 MPa). A nominal stiffness ratio α_{K0}, defined as the ratio between the nominal value of the vertical stiffness (K_{V0}) and the analogous value of the horizontal stiffness (K_{H0}), equal to 1200 is assumed for the isolators, considering a volumetric compression modulus of the rubber equal to 2000 MPa. In Table 1 initial stiffnesses and corresponding equivalent damping coefficients (i.e. C_H and C_V) are reported together with the results of the ULS verifications for the isolators. It is interesting to note that the design of the isolators depends on the condition imposed on the maximum value of the compression axial load (P). Finally, no tensile forces are found in the isolators. The following geometrical and mechanical properties of the HDLRBs are also reported in Table 2: the diameter of the steel layer (D_s) and that of the elastomer (D_e); the total thickness of elastomer (t_e); primary (S_1) and secondary (S_2) shape factors; compression modulus (E_c).

α_{K0}	K_{H0} (kN/cm)	K_{V0} (kN/cm)	C_H (kNs/cm)	C_V (kNs/cm)	γ_s	$\gamma_{tot,max}$	$(P_{cr}/P)_{min}$
1200	81.30	97522	6.47	44.70	0.96	2.85	2.00

Table 1: Mechanical properties of the base-isolation system.

D_s (cm)	D_e (cm)	t_e (cm)	S_1	S_2	E_c (kN/cm^2)
62.00	66.00	25.00	19.22	2.46	55.34

Table 2: Geometrical and mechanical properties of the HDLRBs.

3 FIRE LOADING BEFORE AN EARTHQUAKE AND NUMERICAL RESULTS

Once the fire scenarios, assuming closed openings, have been hypothesized (Figure 1c), temperature is considered uniform in the selected compartment (Figure 1a) in such a way as to be the most severe condition for the fire before an earthquake. Several fire action models can be used to simulate the time-temperature evolution during an actual fire, from the flashover to the full development: conventional fire curves (e.g. the standard ISO-834 curve [18]), in which temperature monotonically increasing with time represents the heating phase only, when the fuel supply is assumed to be inexhaustible; natural fire curves (e.g. the EC1 curve [17]), in which temperature depends on the actual ventilation and fire load in the compartment and the cooling phase is represented, based on the assumption that at a certain point, either the air or the combustible material will become less.

The EC1 parametric fire curve is used in the present study, on the assumption that the fire load of the compartment is completely burnt out. In the heating phase, the gas temperature θ_g(°C)

$$\theta_g = 20 + 1325\left(1 - 0.324e^{-0.2t^*} - 0.204e^{-1.7t^*} - 0.472e^{-19t^*}\right) \tag{1}$$

is a function of a fictitious time t^* obtained considering the time t (in hours) multiplied by a dimensionless parameter equal to

$$\Gamma = \left(O/b\right)^2 \Big/ \left(0.04/1160\right)^2 \tag{2}$$

where O is an opening factor

$$O = A_v h_{eq}^{\ 0.5} \Big/ A_t \tag{3}$$

depending on the total area of vertical openings (A_v), the weighted average of window heights (h_{eq}) and the total area of the compartment (A_t) and b is the thermal absorptivity of

surrounding surfaces of the compartment

$$b = \sqrt{\rho c \lambda} \tag{4}$$

being: ρ the density, c the specific heat and λ the thermal conductivity of boundary of enclosure.

The gas temperature in the cooling phase is given by

$$\begin{aligned} & t^*_{\max} \le 0.5\ h \rightarrow \theta_g = \theta_{\max} - 625\left(t^* - t^*_{\max}\right) \\ & 0.5\ h < t^*_{\max} < 2\ h \rightarrow \theta_g = \theta_{\max} - 250\left(3 - t^*_{\max}\right)\left(t^* - t^*_{\max}\right) \\ & t^*_{\max} \ge 2\ h \rightarrow \theta_g = \theta_{\max} - 250\left(t^* - t^*_{\max}\right) \end{aligned} \tag{5}$$

where the maximum temperature θ_{max} in the heating phase happens for

$$t^*_{\max} = \left(0.2 \cdot 10^{-3} q_{t,d} / O\right) \Gamma \tag{6}$$

being the design fire load density

$$q_{t,d} = q_{f,d}\ A_f / A_t \tag{7}$$

related to the value $q_{f,d}$ corresponding to the surface area of the floor (A_f). Further details on fire modelling can be found in [19].

Finally, the standard ISO-834 curve is defined as [18]

$$\theta_g = 20 + 345 \log_{10}\left(8t + 1\right) \tag{8}$$

where t is expressed in hours.

With reference to the fire scenarios shown in Figure 1, the ISO and EC1 time-temperature curves are compared in Figure 2 in the case of a fire compartment confined to the area of the first level (Figure 2a) and the upper levels (Figure 2b). The combination of fire parameters, for the opened-plan office base-isolated building (see Table 3), results in a temperature of 956 °C and 960 °C in 45 min (i.e. fire resistance R45) and 788 °C and 805 °C in 60 min (i.e. fire resistance R60), on the first level and the upper levels, respectively.

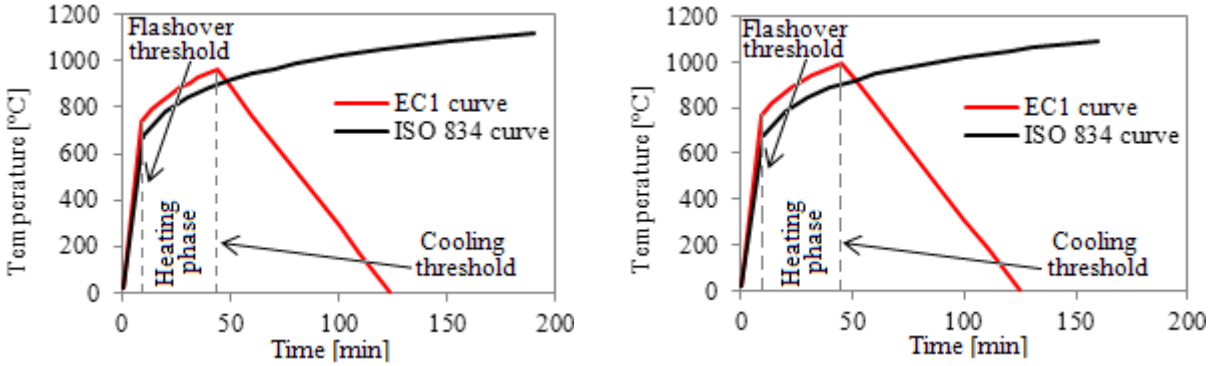

(a) Fire compartment at the 1st level. (b) Fire compartment at the upper levels.

Figure 2: Conventional (ISO 834) and natural (EC1) fire curves.

Fire resistance (minutes)	$q_{f,d}$ (MJ/m^2)	O (m$^{1/2}$)	b (J/m^{2}s$^{1/2}$K)	t^*_{max} (h)
R45	595.60	0.05	1127	1.326
R60	612.00	0.05	1137	1.365

Table 3: Fire parameters in the EC1 time-temperature curve [17].

Once time-temperature curve of the fire compartment is determined with the EC1 model, it becomes possible to evaluate the temperature distribution in the frame members of the test structure at R45 and R60. As an example, thermal mappings of exterior and interior r.c. frame members in the first level of the test structure are plotted in Figure 3, considering a convection factor equal to 25 and an emissivity related to the concrete surface equal to 0.56. In detail, the thermal finite element cross-section model of columns, exposed to fire on one (Figure 3a) and four (Figure 3b) sides, and girders, exposed to fire on one (Figure 3c) and three (Figure 3d) sides, are considered assuming an ambient temperature of 20°C for the un-exposed cross-section sides. As expected, at the end of 45 and 60 minutes of fire exposition, the increase in temperature is greater in the case of cross-sections exposed on four (Figure 3b) or three (Figure 3d) sides than those exposed on one side only (Figures 3a and 3c). Moreover, the temperature profiles highlight a decrease in the maximum value with the time increment from R45 to R60, in accordance with EC1 natural fire curves shown in Figure 2, but the concrete zone damaged by heat is more extended in the case of R60.

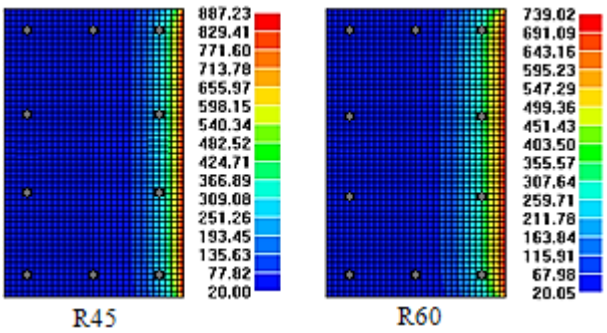

(a) Exterior column exposed to fire on one side.

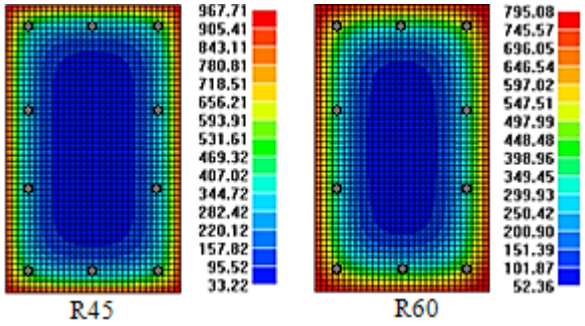

(b) Interior column exposed to fire on four sides.

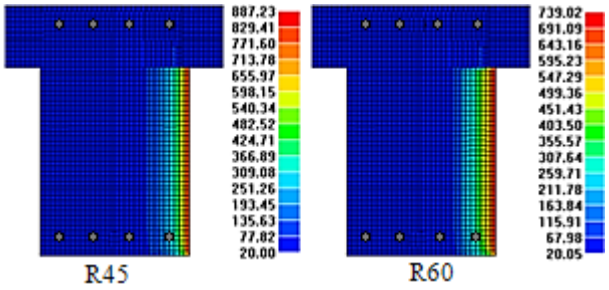

(c) Exterior girder exposed to fire on one side.

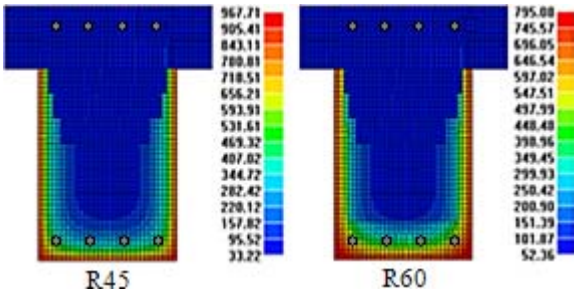

(d) Interior girder exposed to fire on three sides.

Figure 3: Thermal mappings at the 1st level of the test structure.

Subsequently, the residual seismic load capacity of the cross-sections after fire occurrence is evaluated with the 500°C isotherm method of Eurocode 2 [14], in terms of stiffness, strength and ductility. The simplified calculation provides for a reduction of the cross-section size, with respect to a heat damaged zone defined by thermal mappings. Concrete with temperatures exceeding 500°C, corresponding roughly to the thickness of the unconfined zone, is assumed not to contribute, while the residual concrete cross-section retains its initial values of strength and modulus of elasticity. On the other hand, a reduced yield strength of each longitudinal reinforcement bar, in the tension and compression zones of the cross-section, is evaluated on the basis of the steel temperature profile in the centre of the bar [20]. It is worth noting that some of the reinforcing bars may fall outside the reduced cross-section, but they are included in the calculation of the ultimate values of load bearing capacity and curvature ductility, which is evaluated according to the provisions of Eurocode 8 for the assessment of existing buildings [21].

In Figures 4 and 5 flexural stiffness and ultimate ductility on the top side, in the fire-exposed cross-section of r.c. frame members, are reported along the building height, respectively, assuming the direct correspondence between the examined level and the fire compartment. In particular, interior columns (Figures 4a and 5a) and girders (Figures 4b and 5b) are examined at the end of 45 (i.e. F.R45 structure) and 60 (i.e. F.R60 structure) minutes of exposure to fire. As expected, a global mean decrease in stiffness, of about 41% and 28%, and ultimate ductility, of about 16% and 6%, is obtained for the interior columns and girders of the F.R45 structure, respectively, in comparison with the no-fire condition. A further global mean decrease in stiffness, of about 12% and 9%, and ultimate ductility, of about 8%, is obtained after an additional 15 minutes of fire (i.e. F.R60 structure). Further results, which are omitted for the sake of brevity, confirm limited fire effects in the perimeter frame members of all levels where the fire compartment is supposed.

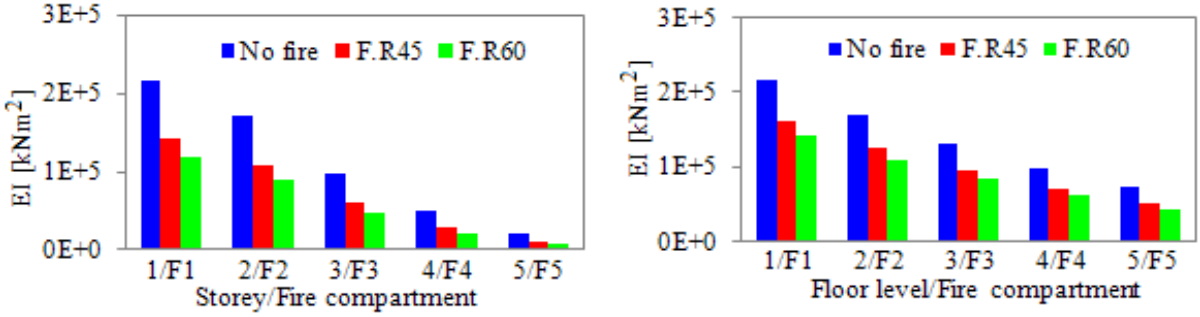

(a) Interior columns. (b) Interior girders.

Figure 4: Flexural stiffness of r.c. frame members exposed to fire.

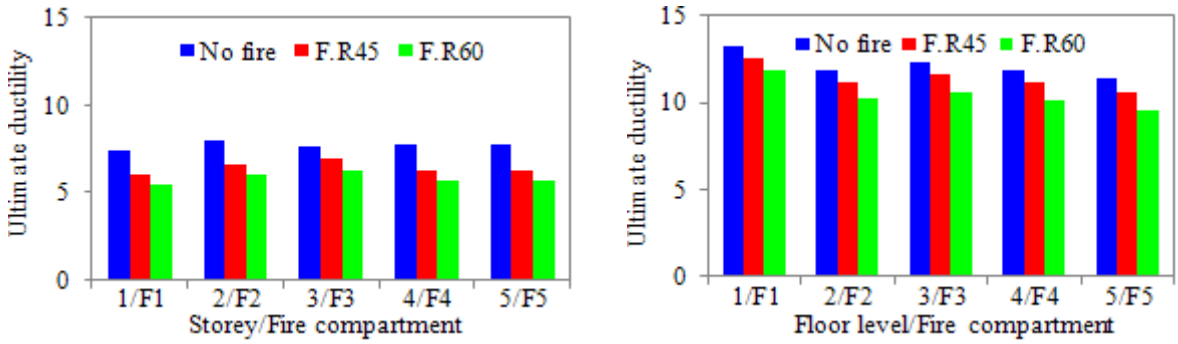

(a) Interior columns. (b) Interior girders (top side).

Figure 5: Ultimate ductility of r.c. frame members exposed to fire.

Finally, analogous results are reported for the ultimate interaction domain between axial load (N_{Rd}) and bending moment (M_{Rd}) of columns (Figure 6) and the ultimate bending moment of girders (Figure 7). For the sake of clarity, only the fire compartment at the first (i.e. F1 in Figures 6a and 7a) and fifth (i.e. F5 in Figures 6b and 7b) level are examined. As can be observed, interior columns exhibit a marked narrowing of their N_{Rd}-M_{Rd} domains, especially for values of the compressive axial load greater than that corresponding to the balanced compressive load. For this axial load, a local reduction in flexural strength, in comparison with the no-fire condition, of about 23% and 36%, at the first storey, and 30% and 47%, at the fifth storey, is found in the F.R45 and F.R60 structures, respectively. On the other hand, a significant decrease in strength is observed on the bottom side of the interior girder 4-5 (see Figure 1a) with a global mean reduction of about 13% and 33% considering the F.R45 and F.R60 structures, respectively.

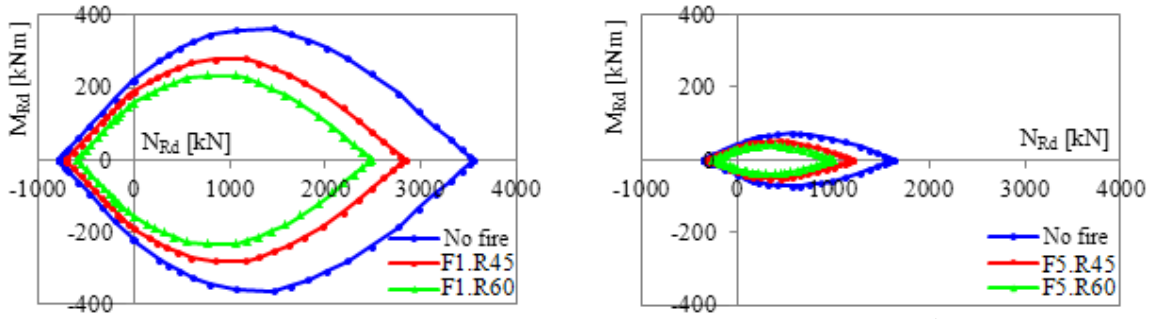

(a) Interior columns (1st storey/F1). (b) Interior columns (5th storey/F5).

Figure 6: Ultimate N_{Rd}-M_{Rd} domains of r.c. columns exposed to fire.

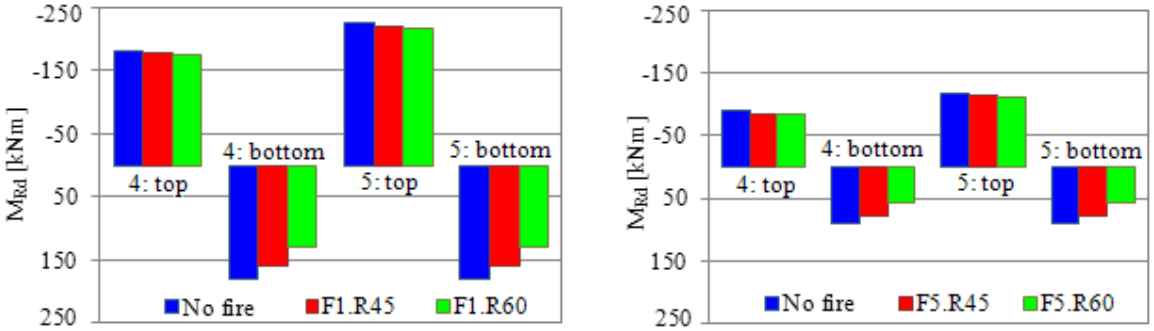

(a) Interior girders (1st floor/F1). (b) Interior girders (5th floor/F5).

Figure 7: Ultimate bending moments of r.c. girders exposed to fire.

4 SEISMIC LOADING FOLLOWING FIRE AND NUMERICAL RESULTS

In order to study the seismic response of the base-isolated r.c. framed building described in Section 2 and damaged by the fire loading proposed in Section 3, near-fault ground motions are considered. Long-duration horizontal pulses due to forward-directivity and fling-step effects characterize these motions [12]. In particular, earthquake rupture towards a site tends to produce a short-duration, but large amplitude, two-sided velocity pulses principally in the horizontal direction normal to the fault strike; on the other hand, fling-step is associated with the permanent displacement that occurs across a ruptured fault and, generally, presents one-sided velocity pulses in the slip parallel direction. Seven near-fault ground motions available in the *Pacific Earthquake Engineering Research center database* [15] have been selected according to the design hypotheses adopted for the test structure (i.e. subsoil class C and high-risk seismic region). For each ground motion attention is focused on the horizontal component showing forward-directivity or fling-step effect [16]. In Table 4 the main data of the selected near-fault ground motions are shown: i.e. date, recording station, component, peak ground acceleration, magnitude, pulse-type and period of the velocity pulse.

Country	Earthquake	Date	Station	Comp.	*PGA*	M_w	Pulse-type	T_p (s)
Taiwan	Chi-Chi	20/09/1999	TCU068	EW	0.566 g	7.3	Fling-step	12.29
USA	Northridge	17/01/1994	Rinaldi	228	0.837 g	6.6	Forward-directivity	1.25
	Superstition Hills	24/11/1987	Parachute	225	0.455 g	6.4	Forward-directivity	2.39
	Cape Mendocino	25/04/1992	Petrolia	090	0.662 g	7.1	Forward-directivity	3.00
Japan	Kobe	16/01/1995	Takatori	090	0.616 g	6.9	Forward-directivity	1.55
Iran	Tabas	16/09/1978	Tabas	TR	0.852 g	7.7	Forward-directivity	6.19
Turkey	Erzincan	13/03/1992	Erzincan	NS	0.515 g	6.7	Forward-directivity	2.70

Table 4: Main data of the selected near-fault ground motions [15, 16].

The corresponding elastic response spectra of normalized acceleration (S_a/g) are plotted in Figure 8, assuming an equivalent viscous damping ratio in the horizontal direction, ξ_H, equal to 10%. The response spectra are compared with the corresponding target NTC08 response spectrum for high-risk seismic region and design subsoil class C adopted for the test structures, assuming PGA_H=0.283g.

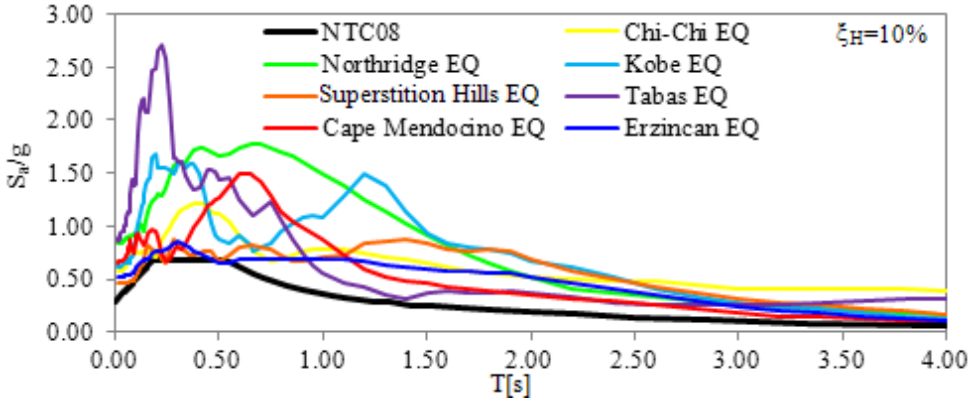

Figure 8: Acceleration (elastic) response spectra.

The r.c. frame members are idealized by means of a two-component model (TCM), constituted of an elastic-plastic component and an elastic component, assuming a bilinear moment-curvature law [22]. The effect of the axial load on the ultimate bending moment of the columns is also considered. At each step of the analysis, the elastic-plastic solution is evaluated in terms of the initial state and the incremental load on the basis of a holonomic law, as a solution of the Haar-Kàrmàn principle [23]. In the Rayleigh hypothesis, the damping matrix of the superstructure is assumed as a linear combination of the mass and stiffness matrices, assuming a viscous damping ratio in the horizontal ($\xi_{S,H}$) and vertical ($\xi_{S,V}$) direction equal to 1% with reference, respectively, to the two fundamental vibration periods $T_{I,H}$ and $T_{I,V}$ reported in Section 3. A two-spring-two-dashpot model (TSTDM), constituted of nonlinear spring acting in parallel with a linear viscous dashpot both in the horizontal and vertical directions, is adopted for modelling a HDLRB [11, 24]. The TSTDM takes into account experimental results, which have pointed out that the horizontal stiffness of a HDLRB (starting from K_{H0}) decreases with increasing vertical load while the corresponding vertical stiffness (starting from K_{V0}) decreases with increasing lateral deformation. Moreover, the equivalent viscous damping ratio of the isolation system is assumed equal to $\xi_{I,H}$=10% and $\xi_{I,V}$=2% with reference to the horizontal motion and the vertical one, respectively.

Incremental dynamic analysis (IDA) of the test structures is carried out by using a series of nonlinear dynamic analyses under the above mentioned set of seven near-fault earthquakes (EQs), each scaled to a submultiple (a_g) of the corresponding PGA value reported in Table 4. Afterwards, a mean of the results separately obtained for these ground motions is calculated. The local damage is evaluated in terms of ductility demand at the critical end sections of girders and columns. The curvature ductility demand is calculated with reference to the two loading directions, assuming as yielding curvature for the columns that corresponding to the axial force due to the gravity loads.

Firstly, mean values of maximum ductility demand for increasing values of the dimensionless acceleration α_a(=a_g/PGA) are plotted in Figure 9, comparing base-isolated structures both in no-fire condition and at the end of 45 (i.e. R45) and 60 (i.e. R60) minutes of fire exposure. More specifically, interior columns (Figures 9a and 9c) and girders (Figures 9b and 9d) are examined, on the assumption that the fire compartment is confined to the area of the first level

(i.e. F1, Figures 9a and 9b) and the first two levels (i.e. F1/2, Figures 9c and 9d). Moreover, the r.c. superstructure of the base-isolated building is assumed to have been previously damaged by fire, with a reduced cross-section (i.e. in the Damaged Stiffness condition, DS), and later repaired, e.g. using jacketing with thin layers of concrete (i.e. in the Repaired Stiffness condition, RS). For all the examined cases, the IDAs were interrupted once the ultimate value imposed on the curvature ductility demand in the r.c. frame members was reached, which occurred at different values of α_a. For this reason, the analyses were repeated assuming the minimum dimensionless acceleration ($\alpha_{a,min}$) for all structures corresponding to the same fire-scenario. As can be observed, an amplification in the structural response of fire-exposed base-isolated structures is obtained for increasing values of α_a. As expected, this result is more evident in the Fi.R60 structures than in the Fi.R45 ones, because the first are characterized by lower strength and ductility. The results also show that the seismic response of the test structures differs in the DS and RS conditions, especially with higher ductility demand of the interior columns (Figures 9a and 9c) in the case when the initial stiffness is restored (i.e. RS condition). It is worth noting that, the IDA was interrupted to $\alpha_{a,min}$=0.395 in the fire scenario F1 (Figures 9a and 9b), while when the fire compartment was confined to the area of the first two levels (Figures 9c and 9d) the IDA was limited to $\alpha_{a,min}$=0.375. Further results, omitted for the sake of brevity, confirm negligible effects at the upper storeys when the fire compartment is supposed at these levels.

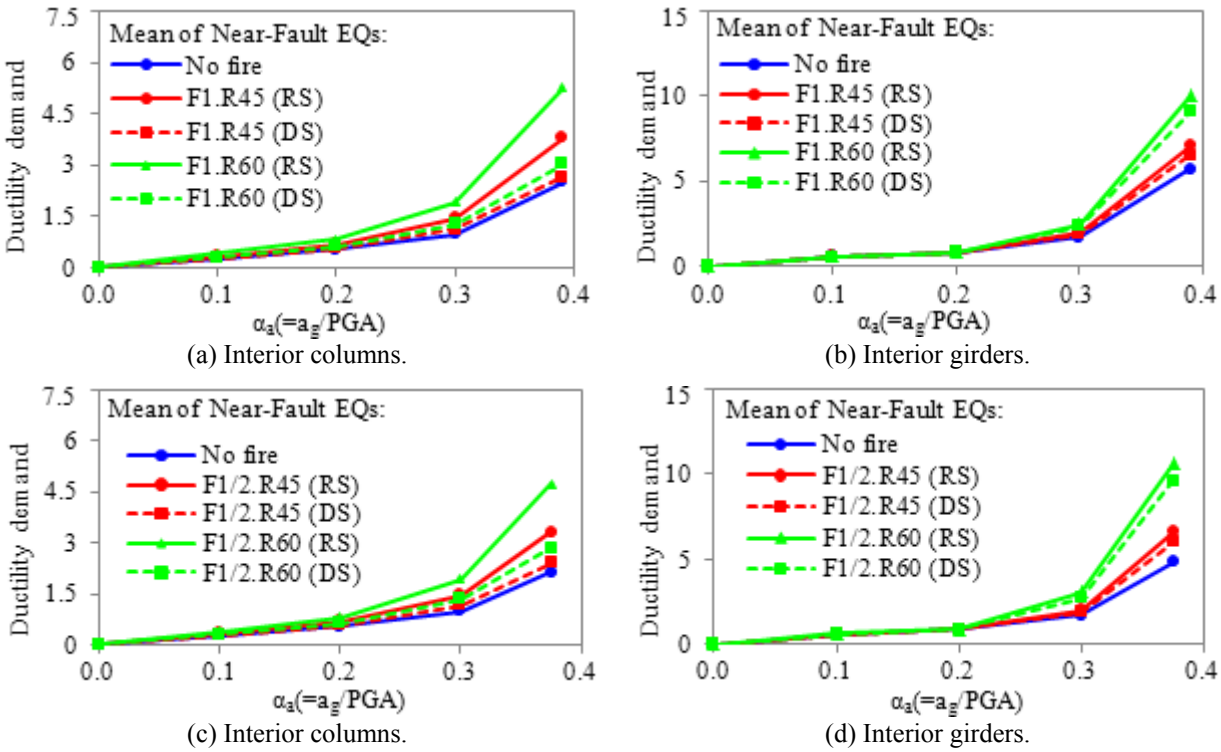

(a) Interior columns. (b) Interior girders.

(c) Interior columns. (d) Interior girders.

Figure 9: Global mean ductility demand for incremental dynamic analysis:
(a) and (b), fire at the 1st level (fire scenario F1); (c) and (d), fire at the 1st and 2nd levels (fire scenario F1/2).

To better clarify the local damage distribution along the building height, mean ductility demand of columns and girders is plotted in Figure 10 at the end of the IDA, in the cases of F1 (i.e. $\alpha_{a,min}$=0.395) and F1/2 (i.e. $\alpha_{a,min}$=0.375) fire scenarios. As can be observed, the pulse-type nature of the horizontal component of near-fault ground motions can induce unexpected ductility demand especially at the lower levels, with an amplification when the fire

compartment at these levels and R60 are assumed. More specifically, the IDAs are interrupted when the ultimate ductility demand of the F1.R60 and F1/2R.60 structures is reached in an interior column on the first storey (Figure 10a) and an interior girder on the second floor (Figure 10d), respectively.

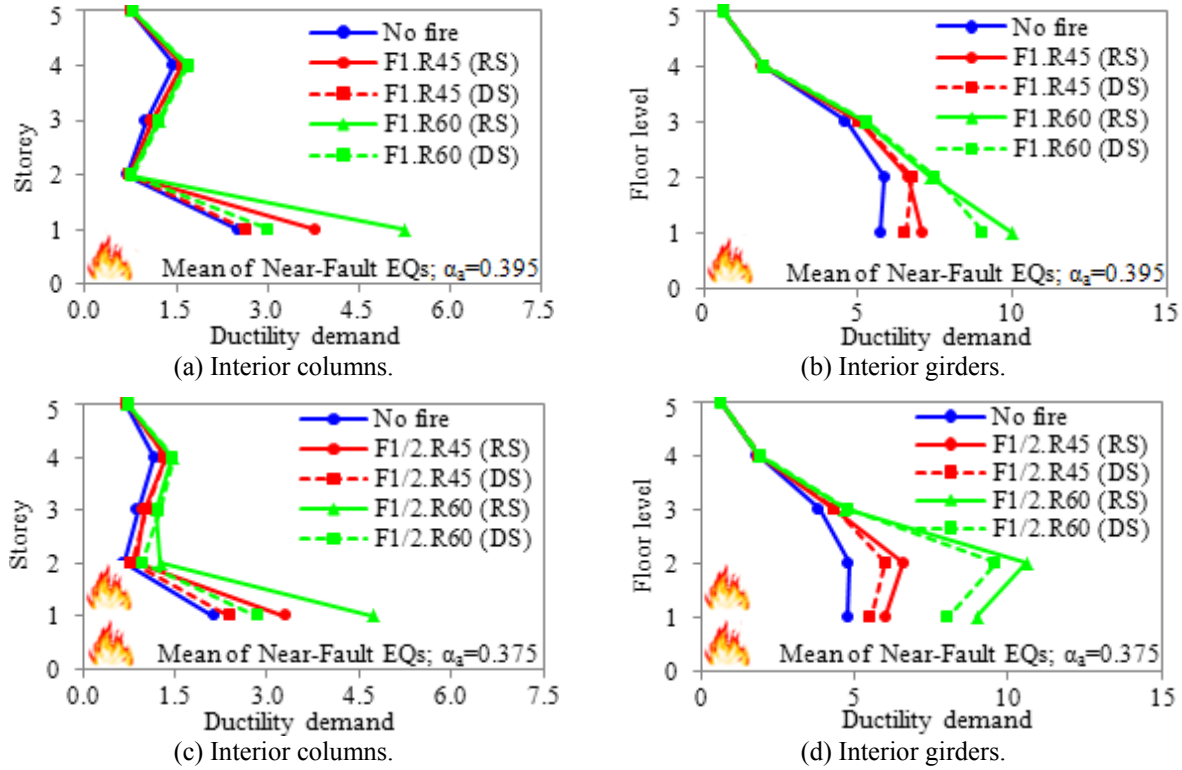

(a) Interior columns. (b) Interior girders.

(c) Interior columns. (d) Interior girders.

Figure 10: Local mean ductility demand at the end of the incremental dynamic analysis: (a) and (b), fire at the 1st level (fire scenario F1); (c) and (d), fire at the 1st and 2nd levels (fire scenario F1/2).

Afterwards, to investigate the effects of forward-directivity and fling-step pulse-type, curves analogous to the previous ones are reported in Figures 11 and 12 with reference to the Superstition Hills and Chi-Chi EQs. Attention is focused on the fire scenario F1, assuming the same final value of the dimensionless acceleration α_a (i.e. $\alpha_{a,min}$=0.395) for both near-fault ground motions. These motions are selected as they are characterized by a comparable value of elastic spectral acceleration (see Figure 8) corresponding to the fundamental vibration period of the base-isolated test structure (i.e. $T_{I,H}$=2.5 s). In all the examined cases, global and local maximum ductility demands of the structures subjected to the Chi-Chi EQ are found to be greater than those observed for the Superstition Hills EQ. This kind of behaviour can be interpreted as an amplification of the inelastic response during the fling-step Chi-Chi EQ due to the long duration of the pulse-velocity (see Table 4).

Finally, taking into account the symmetric plan shown in Figure 1a, the distribution of maximum ductility demand in the exterior and interior frame members is investigated in Figure 13. More specifically, local maximum ductility demand in the columns (Figures 13a and 13c) and girders (Figures 13b and 13d) for the Chi-Chi (Figures 13a and 13b) and Superstition Hills (Figures 13c and 13d) EQs are plotted at the first level where the fire compartment is assumed. Note that the ductility demand increases especially in the frame members exposed on three (i.e. the interior girders 4-5, 5-6, 7-8 and 8-9) and four (i.e. the interior columns 5 and 8) sides. Moreover, among the columns exposed on one side greater ductility demand is obtained in the exterior ones (i.e. 1, 2 and 3).

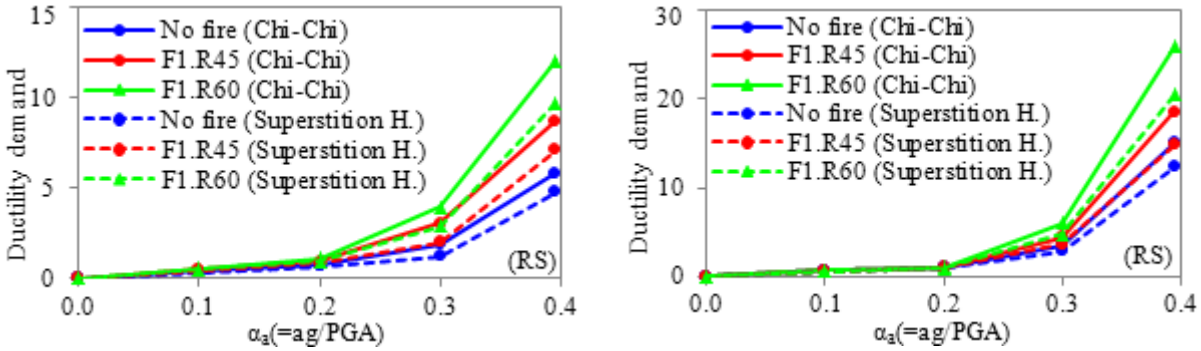

(a) Interior columns. (b) Interior girders.

Figure 11: Global maximum ductility demand for incremental dynamic analysis: fire at the 1st level (fire scenario F1) under Chi-Chi and Superstition Hills EQs.

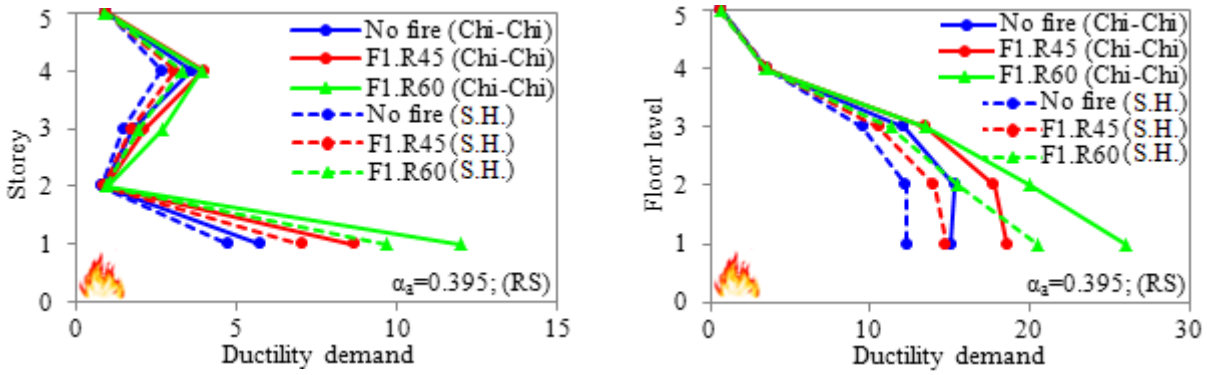

(a) Interior columns. (b) Interior girders.

Figure 12: Local maximum ductility demand at the end of the incremental dynamic analysis: fire at the 1st level (fire scenario F1) under Chi-Chi and Superstition Hills EQs.

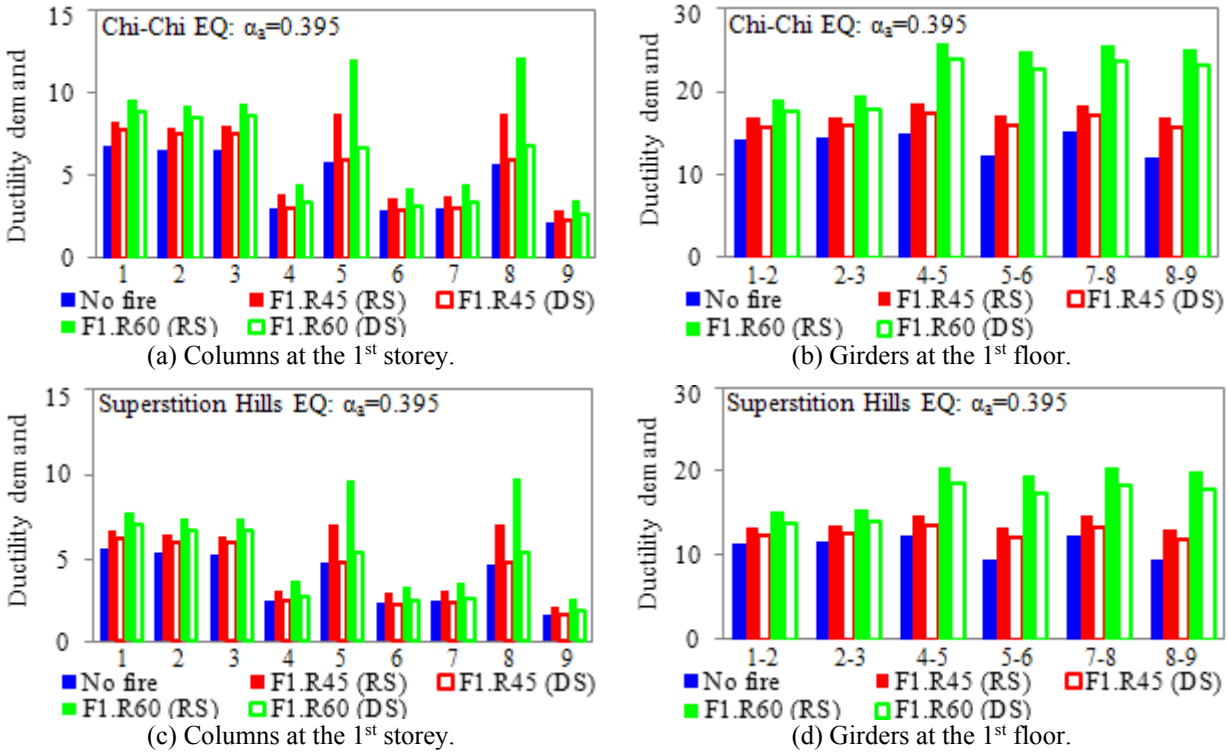

(a) Columns at the 1st storey. (b) Girders at the 1st floor.

(c) Columns at the 1st storey. (d) Girders at the 1st floor.

Figure 13: Local ductility demand in the fire compartment at the end of the incremental dynamic analysis: fire at the 1st level (fire scenario F1) under Chi-Chi (a, b) and Superstition Hills (c, d) EQs.

5 CONCLUSIONS

The nonlinear seismic response of five-storey base-isolated r.c. framed buildings, with fire-protected High-Damping-Laminated-Rubber Bearings, is studied under the horizontal components of seven near-fault ground motions with long-duration velocity pulses due to forward-directivity and fling-step effects. More specifically, the incremental dynamic analysis of base-isolated structures in a no fire situation is compared with that in the event of fire, at 45 (i.e. R45) and 60 (i.e. R60) minutes of fire exposition, assuming both damaged (i.e. DS) and repaired (i.e. RS) stiffness conditions.

The numerical results show that in the case of base-isolated buildings subjected to near-fault motions structural fire safety rules should be taken into account in the design. A significant decrease in stiffness and ultimate values of strength and ductility is obtained in the structural members exposed to fire. Moreover, the pulse-type nature of the horizontal near-fault ground motions induces unexpected ductility demands in the lower levels, which are amplified when the fire compartment is supposed at these levels and R60 is assumed. On the other hand, in all the examined cases the upper storeys are practically independent of this effect. Finally, the ductility demand increases especially in the most fire-exposed r.c. frame members (i.e. the interior girders and columns) in both DS and RS conditions.

ACKNOWLEDGEMENTS

The present work was also financed by Re.L.U.I.S. (Italian network of university laboratories of earthquake engineering), according to "Convenzione D.P.C.–Re.L.U.I.S. 2014–2016, WPI, Isolation and Dissipation".

REFERENCES

[1] C. Scawthorn, J.M. Eidinger, A. Schiff, Fire following earthquake. New York, NY *American Society of Civil Engineers*, 2005.

[2] H. Mostafaei, T. Kabeyasawa, Performance of a six-story reinforced concrete structure in post-earthquake fire. Institute for Research in Construction, *10th Canadian Conference on Earthquake Engineering*, Toronto, Canada, July 25-29, **1**, 481-490, 2010.

[3] B. Behnam, H. Ronagh, Performance of reinforced concrete structures subjected to fire following earthquake. *European Journal of Environmental and Civil Engineering,* **17**(4), 270-292, 2013.

[4] G. Della Corte, R. Landolfo, F.M. Mazzolani, Post earthquake fire resistance of moment resisting steel frames. *Fire Safety Journal*, **38**, 593–612, 2003.

[5] M. Memari, H. Mahmoud, Performance of steel moment resisting frames with RBS connections under fire loading. Engineering Structures, **75**, 126-138, 2014.

[6] E. Nigro, A. Ferraro, G. Cefarelli, R. The influence of fire scenarios on the structural behaviour of composite steel-concrete buildings. *Applied Mechanics and Materials*, **82**, 368-373, 2011.

[7] H. Mostafaei, F. Vecchio, N. Bénichou, Seismic Resistance of Fire-Damaged Reinforced Concrete Columns. *ATC and SEI Conference on Improving the Seismic Performance of Existing Buildings and Other Structures,* San Francisco, California, United States, December 9-11, **1**, 1396-1407, 2009.

[8] H. Mostafaei, Hybrid fire testing for assessing performance of structures in fire - Meth-

odology. Fire Safety Journal, **58**, 170-179, 2013.

[9] H. Mostafaei, Hybrid fire testing for assessing performance of structures in fire - Application. Fire Safety Journal, **56**, 30-38, 2013.

[10] F. Mazza, A. Vulcano, Nonlinear response of r.c. framed buildings with isolation and supplemental damping at the base subjected to near-fault earthquakes. *Journal of Earthquake Engineering*, **13(5)**, 690-715, 2009.

[11] F. Mazza, A. Vulcano, Effects of the near-fault ground motions on the nonlinear dynamic response of base-isolated r.c. framed buildings. *Earthquake Engineering and Structural Dynamics,* **41**, 211-232, 2012.

[12] B.A. Bolt, Seismic input motions for nonlinear structural analysis. *ISET Journal of Earthquake Technology,* **41**(2-4), 223-232, 2004.

[13] Technical Regulations for the Constructions. Italian Ministry of the Infrastructures, January 14, 2008 (in Italian).

[14] Eurocode 2. Design of concrete structures – Part 1-2: General rules, structural fire design. *C.E.N., European Committee for Standardization*, December 2004.

[15] Pacific Earthquake Engineering Research Center database. peer.berkeley.edu/smcat /search.html.

[16] E. Kalkan, S.K. Kunnath, Relevance of absolute and relative energy content in seismic evaluation of structures. *Advances in Structural Engineering*, **11**(1), 17-34, 2008.

[17] Eurocode 1. Actions on structures – Part 1-2: General actions, actions on structures exposed to fire. *C.E.N., European Committee for Standardization*, October 2004.

[18] ISO 834 International Standard, Fire resistance tests, ISO 834-1 Test conditions. *Provided by IHS under license with ISO: 31*, Genève, Switzerland, 1999.

[19] F. Mazza, A. De Luca, Seismic vulnerability in case of fire of existing r.c. framed buildings: modelling and nonlinear dynamic analysis. *COMPDYN 2015, 5th ECCOMAS Thematic Conference on Computational Methods in Structural Dynamics and Earthquake Engineering*, Crete Island, Greece, May 25–27, paper n. 491, 2015.

[20] F. Mazza, M. Fiore, Comparative study of the wind and earthquake dynamic responses of fire exposed steel framed buildings. *COMPDYN 2015, 5th ECCOMAS Thematic Conference on Computational Methods in Structural Dynamics and Earthquake Engineering*, Crete Island, Greece, May 25–27, paper n. 490, 2015.

[21] Eurocode 8. Design of structures for earthquake resistance – Part 3: Assessment and retrofitting of buildings. *C.E.N, European Committee for Standardization*, June 2004.

[22] F. Mazza, M. Mazza, Nonlinear analysis of spatial framed structures by a lumped plasticity model based on the Haar-Kàrmàn principle. *Computational Mechanics*, **45**, 647-664, 2010.

[23] F. Mazza, A distributed plasticity model to simulate the biaxial behaviour in the nonlinear analysis of spatial framed. *Computers and Structures*, **135**, 141-154, 2014.

[24] F. Mazza, M. Mazza, A. Vulcano, Nonlinear Dynamic Response of R.C. Buildings with Different Base-Isolation Systems Subjected to Horizontal and Vertical Components of Near-Fault Ground Motions. *The Open Construction & Building Technology Journal,* **6**, 373-383, 2012.